Available online at www.sciencedirect.com
SCIENCE DIRECT®
Journal of Nuclear Materials 348 (2006) 45–50
journal of nuclear materials
www.elsevier.com/locate/jnucmat

Equilibria in the Zr–Hf–Sn system in the region up to 37.5 at.% Sn

D.H. Ruiz [a], A.M. Monti [a], M. Ortiz Albuixech [a], L.M. Gribaudo [a,b,*]

[a] *Departamento Materiales, Centro Atómico Constituyentes, Comisión Nacional de Energía Atómica, Avda. Gral. Paz 1499, B1650KNA San Martín, Argentina*
[b] *Consejo de Investigaciones Científicas y Tecnológicas, Avda. Rivadavia 1917, C1033AAJ, Buenos Aires, Argentina*

Received 22 June 2005; accepted 27 August 2005

Abstract

Phase equilibria in the zirconium–hafnium–tin system between the Mn_5Si_3-type intermetallic and the (Zr,Hf) rich solid solution were determined studying three alloys of selected compositions in the region up to 37.5 at.% Sn. Phase characterizations were made on heat-treated specimens at 900 and 1100 °C by metallographic observations, X-ray diffraction diagrams and electron microprobe analysis. Lattice parameters of the phases in equilibrium were calculated. General sketches of equilibria and phase boundaries at the mentioned temperatures were outlined from the obtained results.

PACS: 61.66.Dk; 61.66.Fn; 81.30.Bx

1. Introduction

Zirconium alloys are commonly employed in the nuclear industry. The one known as Zircaloy, commonly used for cladding tubes and other components, has tin as the main alloying component. On the other hand, hafnium (with zirconium additions) is employed for control bars in some nuclear reactors such as the PHWR type Atucha I and Atucha II in Argentina. These reasons have motivated the study of the ternary system zirconium–hafnium–tin, particularly in the transition metals rich part. To the authors knowledge, no reports on this subject are nowadays available.

The three binary systems which limit the ternary alloy under examination, i.e. Zr–Sn, Zr–Hf and Hf–Sn, have been relatively well studied and assessed in the past [1–3]. Temperature–composition diagrams of these systems have been lately compiled in 'Binary Alloy Phase Diagrams' edited by AMS International [4].

Early work done on the Zr–Ti–Sn system [5,6] has shown that the Mn_5Si_3-type intermetallic appears as a compound of formula $(Ti_xZr_{1-x})_5Sn_3$ interchanging completely Ti (or Zr) by Zr (or Ti). This intermetallic can be in equilibrium with different phases depending on the temperature and the global composition of the alloy.

* Corresponding author: Fax: +54 11 6772 7363.
E-mail address: gribaudo@cnea.gov.ar (L.M. Gribaudo).

0022-3115/$ - see front matter
doi:10.1016/j.jnucmat.2005.08.014

In this paper, the ternary Zr–Hf–Sn is experimentally studied in the zone comprised between 0 and 37.5 at.% Sn, where this kind of intermetallic could appear in stable equilibria with the transition metal solid solution. It was assumed that the hexagonal $D8_8$ intermetallic Mn_5Si_3-type, which is a stable phase in each limit binary Zr–Sn and Hf–Sn diagram (Zr_5Sn_3 and Hf_5Sn_3, respectively) presents continuity when both transition metals are interchanged in the lattice.

Experimental results of the characterization and composition of the phases in equilibrium at 900 and 1100 °C of the system Zr–Hf–Sn for an area of the Gibbs triangle bounded by the Hf–Zr side and the boundary passing through the compounds Hf_5Sn_3 and Zr_5Sn_3, are presented and discussed in this work. As a summary, partial isothermal sections have been established and are reported in the present paper.

2. Experimental methods

Three alloys were elaborated by melting the metal components, a hafnium rich alloy taken from a piece of a control bar which contains 3.5 wt% of zirconium (principal impurities oxygen and tantalum, lower than 1500 and 100 ppm, respectively), pure zirconium (purity higher than 99.85 wt%, principal impurities 420 ppm of oxygen and 600 ppm of iron) and tin (purity 99.999 wt%), in a non-consumable tungsten electrode arc furnace with a copper crucible and under high purity argon atmosphere (99.999%), using titanium as an oxygen getter. The 15 g buttons were turned over inside the furnace and re-melted four times in order to achieve homogeneity. The alloy compositions are reported in Table 1.

Samples of the arc-melted buttons were wrapped in tantalum foil, sealed in evacuated quartz tubes, annealed 1440 h at (1100 ± 2) °C or 2440 h at (900 ± 2) °C and water-quenched without breakage of the tubes at the end of the treatments. The surfaces of the samples were mechanically ground. No chemical etching was performed.

Table 1
Compositions of the investigated Zr–Hf–Sn alloys in at.%

Alloy	Zr	Hf	Sn
A	67.8	12.4	19.8
B	41.7	38.9	19.4
C	16.5	64.4	19.1

Phase characterizations were made initially by optical microscopy in a Reichert-MEF II equipment. For the final phase characterization, X-ray diffraction patterns were obtained from massive and powder samples in a PW3710 Philips equipment using CuKα radiation.

Compositions of phases were determined by wavelength dispersive electron-probe microanalysis in a CAMECA SX50 equipment. The quantitative compositional analysis was performed under an accelerating potential of 20 kV. The equipment was recalibrated before each analysis session and the metallic elements were determined simultaneously. Two methods were applied: (1) on a number of convenient points of a determined massive phase and (2) on many points by a scanning mode analysis crossing different phases. The latter mode is useful to delineate qualitatively and semi-quantitatively the presence of small size or slender phases. It consists in measuring compositions on 100 or 200 aligned points consecutively at steps of 1 μm each. Raw data are correspondently placed on the compositional tie-lines for two-phase equilibria or triangles for three-phase equilibria. Thus the limiting equilibrium phases in the analyzed sample can be identified, and eventually their real compositions can be extrapolated. The criterion used to assign the final chemical composition to the measured phase, was to take into account only the extreme values of each generated geometrical sector (triangles in a three-phase or bands in two-phase domains).

Lattice parameters of the phases were obtained by least-square fittings or refinement of room temperature diffraction data on massive samples using the Rietveld method [7–9].

3. Results

3.1. Microstructures

Fig. 1 shows microstructures of as-cast and heat-treated alloys A and C at 1100 °C. In the as-cast conditions the dendritic body has the acicular microstructure characteristic of the β^t phase [6]. The phase β^t corresponds to the bcc phase formed as the first solidified phase, that after quenching, has the hcp structure of the α phase. The needles are better observed in the hafnium rich alloy C. In the 1100 °C heat-treated alloys the relative phase volumes and morphology have changed by coarsening. The 900 °C heat-treated specimens have essentially similar morphologies to those of 1100 °C but

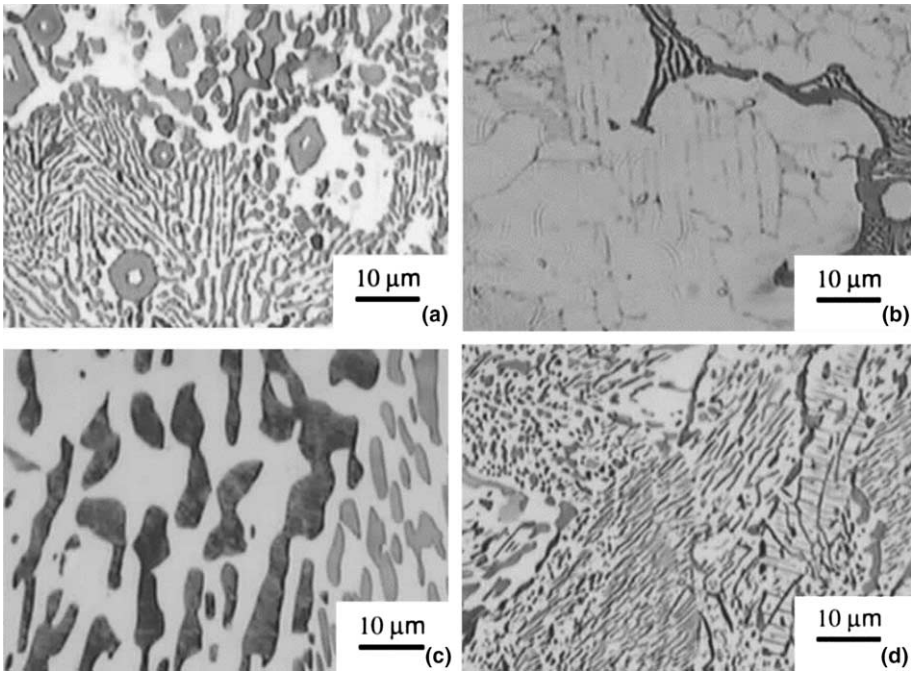

Fig. 1. Microstructures of alloys A and C in as-cast and heat-treated (1100 °C) conditions. (a) A, as-cast; (b) C, as-cast; (c) A, heat-treated; (d) C, heat-treated. Solid solution and intermetallic in light and dark grey, respectively.

thinner microstructures. It is noted that no acicular morphology was perceived at these temperatures for any of the alloys, the solid solution phase is α-(Zr,Hf,Sn).

3.2. X-ray diffraction patterns

A typical X-ray diffraction diagram of these alloys is shown in Fig. 2. It corresponds to alloy A treated at

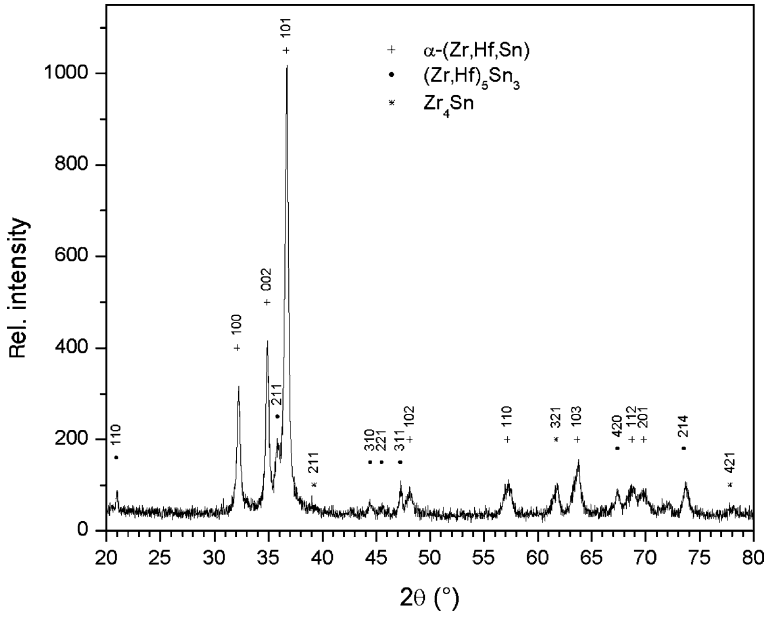

Fig. 2. Experimental X-ray diffraction diagram of alloy A heat-treated at 1100 °C. Modelled peak positions and Miller indices of the identified phases are included.

Table 2
Lattice parameters (nm) of the equilibrium phases

Phase	Heat-treated at 1100 °C			Heat-treated at 900 °C		
	A	B	C	A	B	C
α-(Zr,Hf,Sn)	$a = 0.3219$ $c = 0.5142$	$a = 0.31932$ $c = 0.50987$	$a = 0.31817$ $c = 0.5082$	$a = 0.3217$ $c = 0.5137$	$a = 0.32012$ $c = 0.5096$	$a = 0.3182$ $c = 0.5069$
$(Zr_xHf_{1-x})_5Sn_3$	$a = 0.8481$ $c = 0.581$	$a = 0.8439$ $c = 0.5791$	$a = 0.8418$ $c = 0.5745$	$a = 0.8470$ $c = 0.5791$	$a = 0.8449$ $c = 0.5781$	$a = 0.8407$ $c = 0.5752$
Zr_4Sn	$a = 0.562$	–	–	*	–	–

* Not detected.

1100 °C where the major component phases are the hcp α-(Zr,Hf,Sn) solid solution and the hexagonal compound $(Zr_xHf_{1-x})_5Sn_3$. A set of weak peaks can be assigned to the Zr_4Sn intermetallic. Some discrepancies of peak intensities, attributed to the presence of crystallographic texture in the massive specimens, were found when comparing the experimental and the simulated diagrams. On the other hand, in alloys B and C treated at 1100 °C and the three alloys treated at 900 °C, the phases α-(Zr,Hf,Sn) and $(Zr_xHf_{1-x})_5Sn_3$ were only found.

The lattice parameters of the equilibrium phases in alloys A–C at 1100 °C are presented in Table 2. They were determined from diffraction diagrams obtained from massive samples and applying the Rietveld method. Lattice parameters of alloys heat-treated at 900 °C are similar.

3.3. Phase compositions

The results of compositions of the α-(Zr,Hf,Sn) solid solution and the $(Zr_xHf_{1-x})_5Sn_3$ intermetallic

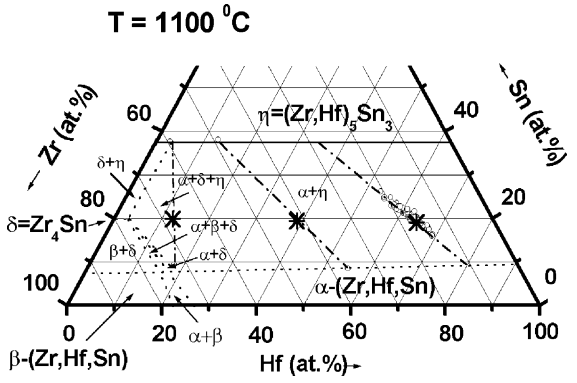

Fig. 3. Isothermal section of the Zr–Hf–Sn system at 1100 °C, axes in at.%, (○) composition determination, (✱) global composition of alloys. Solid lines for experimental boundaries, dashed-dotted lines for tie-lines, dashed lines for predicted phase boundaries.

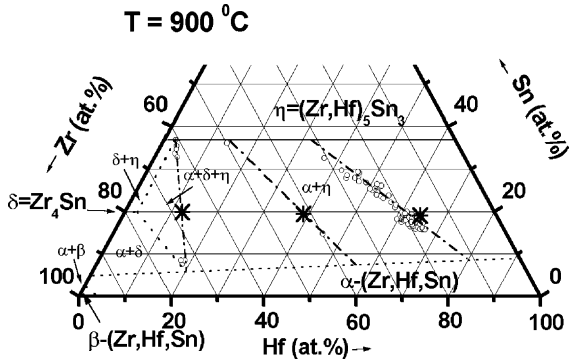

Fig. 4. Isothermal section of the Zr–Hf–Sn system at 900 °C, axes in at.%, (○) composition determination, (✱) global composition of alloys. Solid lines for experimental boundaries, dashed-dotted lines for tie-lines, dashed lines for predicted phase boundaries.

Table 3
Composition of the conjugated phases in the alloys (at.%) heat treated at 1100 °C

Alloy	α-(Zr,Hf,Sn)			$(Zr_xHf_{1-x})_5Sn_3$		
	Zr	Hf	Sn	Zr	Hf	Sn
A*	73.3	18.8	7.9	59.4	3.1	37.5
B	36.3	54.9	8.8	48.8	13.7	37.5
C	10.4	79.7	9.9	28.1	34.4	37.5

* The equilibrium involves also the Zr_4Sn intermetallic whose composition has not been determined.

Table 4
Composition of the conjugated phases in the alloys (at.%) heat treated at 900 °C

Alloy	α-(Zr,Hf,Sn)			$(Zr_xHf_{1-x})_5Sn_3$		
	Zr	Hf	Sn	Zr	Hf	Sn
A*	74.8	19.4	12.9	60.4	2.1	37.5
B	36.3	56.2	7.5	50.1	12.4	37.5
C	12.9	78.5	8.6	31.0	31.5	37.5

* The equilibrium involves also the Zr_4Sn intermetallic whose composition has not been determined.

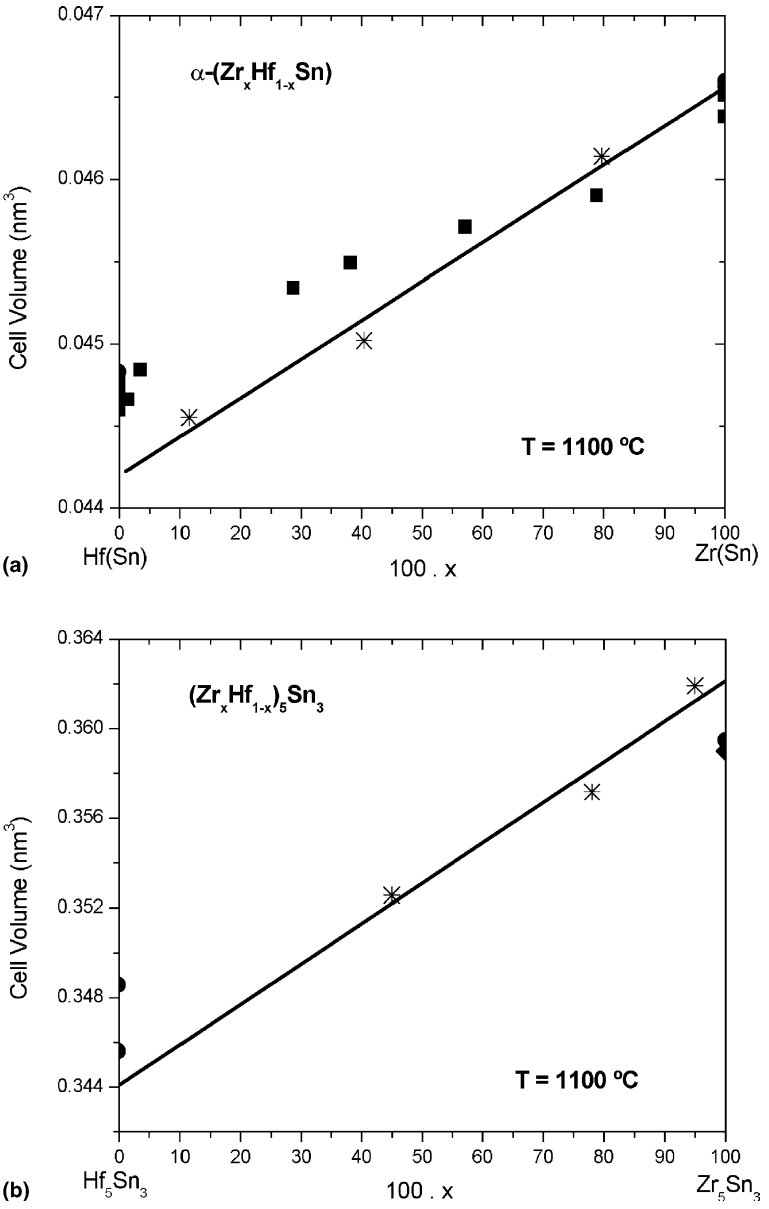

Fig. 5. Experimental cell volumes of the α-(Zr,Hf,Sn) phase and the $(Zr_xHf_{1-x})_5Sn_3$ intermetallic, (✱) present work, (●) Ref. [10], (■) Ref. [11], (◆) Ref. [12]. Data taken from Ref. [11] have been slightly modified in order to include the effect of Sn on the lattice parameters of α-(Zr,Hf,Sn). Vegard's law (in lines).

measured in the microprobe equipment are plotted in the proposed equilibrium diagrams presented in Figs. 3 and 4 for 1100 and 900 °C, respectively. All the measurements obtained by the scanning mode of analysis show the dispersion of compositions which is a characteristic of a very fine microstructure. The measured global compositions of alloys are also indicated in the figures.

The compositions of conjugated phases in equilibrium are reported in Tables 3 and 4. They are taken from tie-lines which have been drawn considering extrapolated results of the microanalysis and phase boundaries obtained from data of the binary diagrams.

3.4. Cell volumes of α-(Zr,Hf,Sn) and $(Zr_xHf_{1-x})_5Sn_3$

Fig. 5(a) and (b) show the cell volumes of the equilibrium phases, solid solution and intermetallic

respectively, at 1100 °C and different compositions of the interchangeable transition element. The compositions are taken from the evaluated tie-lines. The straight lines on the figures correspond to the Vegard's law drawn from the results obtained in the present work. Data taken from the literature are also included.

4. Discussion and conclusions

The isothermal sections at 1100 °C and 900 °C were drawn from combined microprobe and X-ray diffraction analysis of the alloys together with the extrapolated boundaries of the binary systems. The univariant reaction involving $(Zr_xHf_{1-x})_5Sn_3$, Zr_4Sn and α-(Zr,Hf,Sn) was clearly defined at 1100 °C, the Zr_4Sn being present in a small amount. At 900 °C the time of the heat-treatments was not sufficient to obtain the full equilibrium in the alloys and the intermetallic Zr_4Sn was, therefore, not determined by X-ray analysis. The time required for its formation, as compared to 1100 °C, would be about 3.5 times longer (more than 5000 h) after a rough estimation using interdiffusion data from the Zr–Hf system (85 at.% Zr) [13].

It is important to remark that the fulfillment of the Vergard law in the $(Zr_xHf_{1-x})_5Sn_3$ intermetallic, assures the correct evaluation of the compositions of the phases in equilibrium. In addition, the hypothesis about the interchangeability of both transition elements Zr and Hf in the intermetallic is confirmed.

Boundaries of the stable phases in the diagram were drawn considering different degrees of accuracy based on experimental determinations. Those named 'predicted' have been suggested by extrapolation of the binaries or partial results.

Compositions of the $(Zr_xHf_{1-x})_5Sn_3$ intermetallic and the α-(Zr,Hf,Sn) solution phase were presented for one univariant and two bivariant equilibria at 1100 and 900 °C for the three studied alloys.

Acknowledgement

This work has been supported by CNEA – Argentina (P5-PID-35-2-01), CONICET – Argentina (PIP 1064-98) and ANPCyT – Argentina (PICT 12-06164-99).

References

[1] J.P. Abriata, J.C. Bolcich, D. Arias, Bull. Alloy Phase Diagrams 4 (1983) 147.
[2] H. Okamoto, submitted to the APD Program, published in [4], p. 2111.
[3] J.P. Abriata, J.C. Bolcich, H.A. Peretti, Bull. Alloy Phase Diagrams 3 (1982) 29.
[4] T.B. Massalski, H. Okamoto, P.R. Subramanian, L. Kacprzak, Binary Alloy Phase Diagrams, 2nd Ed., ASM International, Metals Park, OH, 1996.
[5] H. Nowotny, H. Auer-Welsbach, J. Buiss, A. Kohl, Monatsh. Chem. 90 (1959) 15.
[6] S.F. Aricó, L.M. Gribaudo, J. Nucl. Mater. 288 (2001) 217.
[7] H.M. Rietveld, J. Appl. Crystallogr. 2 (1969) 65.
[8] L. Lutterotti, P. Scardi, P. Maistrelli, J. Appl. Crystallogr. 25 (1992) 459.
[9] W. Kraus, G. Nolze, U. Müller, PowderCell Program, Federal Institute for Materials Research and Testing Laboratory, BAM-V-13 X-Ray Diffraction and Microanalysis, Berlin, 1998.
[10] P. Villars, L.D. Calvert, Pearson's Handbook of Crystallographic Data for Intermetallic Phases, 2nd Ed., ASM International, Materials Park , OH 44073, 1991.
[11] L. Ming, M.H. Manghnani, K.W. Katahara, J. Appl. Phys. 52 (1981) 1332.
[12] W. Rossteutscher, K. Schubert, Z. Metallkd. 56 (1965) 813.
[13] D. Ansel, A.M. Boliveau, J. Debuigne, Scr. Mater. 34 (1996) 749.